Desorption of hydroxyl radicals in the vacuum ultraviolet photolysis of amorphous solid water at 90 K

Tetsuya Hama,[1] Akihiro Yabushita,[1] Masaaki Yokoyama,[1] Masahiro Kawasaki,[1,a)] and Stefan Andersson[2]
[1]*Department of Molecular Engineering, Kyoto University, Kyoto 615-8510, Japan*
[2]*Leiden Observatory, Leiden University, P.O. Box 9513, 2300 RA Leiden, The Netherlands and Gorlaeus Laboratories, Leiden Institute of Chemistry, Leiden University, P.O. Box 9502, 2300 RA Leiden, The Netherlands*

(Received 16 January 2009; accepted 9 July 2009; published online 6 August 2009)

We have studied the desorption dynamics of OH radicals from the 157 nm photodissociation of amorphous solid water (ASW) as well as H_2O_2 deposited on an ASW surface at 90 K. The translational and internal energy distributions of OH were measured using resonance-enhanced multiphoton ionization methods. These distributions are compared to reported molecular dynamics calculations for the condensed phase photodissociation of water ice and also reported results for the gas phase photodissociation of H_2O at 157 nm. We have confirmed that OH radicals are produced from two different mechanisms: one from primary photolysis of surface H_2O of ASW, and the other being secondary photolysis of H_2O_2 photoproducts on the ASW surface after prolonged irradiation at 157 nm. © *2009 American Institute of Physics*. [DOI: 10.1063/1.3191731]

I. INTRODUCTION

Experimental and theoretical studies on the effects of radiolysis by UV photons on pure or mixed water have been extensively reported because of its importance to reaction dynamics and kinetics, atmospheric chemistry, and astrophysics.[1–3] The first absorption band of water ice (the $\tilde{A}\ ^1B_1 - \tilde{X}\ ^1A_1$ transition) has significant cross section in the 130–165 nm range,[4] and photodissociation of H_2O in the gas phase involves two primary processes in the first absorption continuum,[5,6]

$$H_2O + h\nu \rightarrow H_2 + O(^1D), \tag{1}$$

$$H_2O + h\nu \rightarrow H + OH. \tag{2}$$

The effects of irradiating pure water ice by UV photons have received much experimental study.[7–10] Gerakines *et al.*[7] observed OH, HO_2, and H_2O_2 as products in the condensed phase through infrared spectroscopy after amorphous solid water (ASW) at 10 K was exposed to UV light ($\lambda > 110$ nm). Ghormley and Hochanadel[8] reported the formation of H, OH, and H_2O_2 in the condensed phase after Xe-discharge flash photolysis of crystalline ice at 263 K. Experimental works on photon- or electron-stimulated desorption of species from water ice were also reported. Westley *et al.*[9,10] investigated the absolute desorption yield from water ice at 35–100 K under irradiation with Lyman-α photons of 10.2 eV. Kimmel and co-workers[11,12] used resonance-enhanced multiphoton ionization (REMPI) methods to study the electron-stimulated desorption of D and O atoms and D_2 molecules from amorphous D_2O. In addition to the dissociation of water molecules, secondary reactions at the ASW/vacuum interface are also important for the desorption from ASW. Petrik *et al.*[13] found that electron-stimulated desorption of O_2 occurs via the secondary processes of OH, HO_2, and H_2O_2 products at the surface/vacuum interface of ASW. Yabushita *et al.*[14–16] observed that the photodesorption of cold and hot H_2 from ASW is induced by the surface reactions of H atoms produced in reaction (2).

To understand the photolysis of ASW comprehensively, it is crucial to reveal the contribution of secondary photoproducts. By direct detection of photodesorbed species, the characteristic behavior of ice photolysis may be investigated. Since OH photoproducts are readily trapped in the ice matrix, H_2O_2 was produced on the water ice surface at 90 K presumably due to recombination of photolytically produced OH,[17]

$$OH + OH \rightarrow H_2O_2. \tag{3}$$

H_2O_2 formed via reaction (3) could be subsequently photodissociated to generate OH as a secondary photoproduct,

$$H_2O_2 + h\nu \rightarrow 2OH. \tag{4}$$

Molecular dynamics (MD) calculations by Andersson and co-workers[18,19] predicted the probabilities of H atom, OH, and H_2O desorption from the vacuum ultraviolet (vuv) photolysis of ASW. Öberg *et al.*[20] used a vuv lamp emitting in the range of 7.0–10.5 eV to irradiate ices at surface temperatures in the range of 18–100 K and detected desorbing species such as H_2O, OH, H_2, and O_2. However, experimental results on the details of the mechanism of photodesorption and the kinetic and internal energy distributions of the OH products have not yet been reported. In the present study, we have investigated translational and internal energy distributions of photodesorbed OH radicals following the 157 nm photodissociation of ASW and H_2O_2 at 90 K to reveal the desorption dynamics of OH radicals,

a)Author to whom correspondence should be addressed. Electronic mail: kawasaki@photon.mbox.media.kyoto-u.ac.jp.

$$H_2O(ads) + h\nu(157\ nm) \rightarrow H(\mathbf{i}) + OH(\mathbf{i}), \quad (5)$$

$$H_2O_2(ads) + h\nu(157\ nm) \rightarrow 2OH(\mathbf{i}). \quad (6)$$

The available energies in units of kcal/mol for reactions (5) and (6) at 157 nm are $E_{avail}(5)=51.2$ and $E_{avail}(6)=115.9$ kcal/mol. In this work, the notation "ads" stands for condensed phase or adsorbed state, and the thermodynamic data for adsorbed species are taken from those for the solid phase. The notation **i** stands for species at the ASW/vacuum interface, and for these species we use the gas phase thermodynamics data.[21,22] Based on the present results we have proposed two OH formation mechanisms, reactions (5) and (6). Reaction (6) is appreciable after prolonged vuv irradiation on ASW.

II. EXPERIMENTAL

A. Apparatus and preparation of ice films

Surface photodissociation of ASW at 90 K was carried out in a high vacuum chamber, which was equipped with two turbo molecular pumps, a pulsed molecular beam, an excimer laser, and a dye laser. The experimental details are described elsewhere.[23] In brief, a vacuum chamber was evacuated to a base pressure of 10^{-8} Torr using two turbomolecular pumps in tandem (Shimadzu, 800 and 50 L s^{-1}). A circular sapphire substrate sputter coated with a thin polycrystalline film of Au(111) was supported in the center of the chamber by a liquid-nitrogen-cooled manipulator connected to an *X-Y-Z* stage.[24] The temperature of the substrate was controlled to within 1 K. The controller was composed of an alumel-chromel resistance thermometer with cooling by liquid nitrogen and heating from a 0.35 mm diameter tantalum filament attached to the substrate. The ASW film was prepared by back-filling deposition of water vapor onto the substrate at 90 K for 60 min by a pulsed nozzle (general valve) at the rate of 10 Hz and at 30 Torr stagnation pressure of water vapor. In order to spread water vapor all over the chamber, a flat plate was attached in front of the pulse nozzle. The exposure was typically 1800 L (1 $L=1\times10^{-6}$ Torr s). Unfocused 157 nm laser (Lambda Physik, OPTexPro) radiation was incident at an angle of about 80° to the surface normal on the ice surface at a fluence of <0.1 mJ cm^{-2} $pulse^{-1}$. Neutral OH photofragments produced by the photolysis laser were subsequently ionized at a distance of $r=2$ mm from the substrate surface, as shown in the schematic diagram of the experimental arrangement (Fig. 1). The OH photofragments were ionized by (2+1) REMPI via the $D\ ^2\Sigma^-(v'=0) \leftarrow X\ ^2\Pi(v''=0)$ transition at 243.5–244.5 nm and via the $D\ ^2\Sigma^-(v'=1) \leftarrow X\ ^2\Pi(v''=0)$ and $3\ ^2\Sigma^-(v'=0) \leftarrow X\ ^2\Pi(v''=1)$ transitions at 237.5–237.7 nm, and collected with a small mass spectrometer aligned perpendicular to the ice surface. Two-photon absorption cross sections reported by Greenslade *et al.*[25] allow us to estimate the ratio of $(v''=1)/(v''=0)$. Radiation at 237–245 nm was produced by a Nd^{3+}:yttrium aluminum garnet pumped dye laser (Lambda Physik, SCANmate) with subsequent frequency doubling and mixing in BBO crystals. OH can be formed via two different pathways: (a) by direct photolysis of ASW, reaction (5), and (b) by photolysis of H_2O_2 photoproducts after prolonged irradiation of ice, reaction (6). To suppress the contribution of OH photoproducts formed by the secondary photolysis of H_2O_2 products on the surface of ASW via reaction (6), the ASW surface was continually refreshed by intermissive exposure to H_2O vapor. The pulsed valve was opened after each laser shot so as to deposit a fresh layer of ASW.

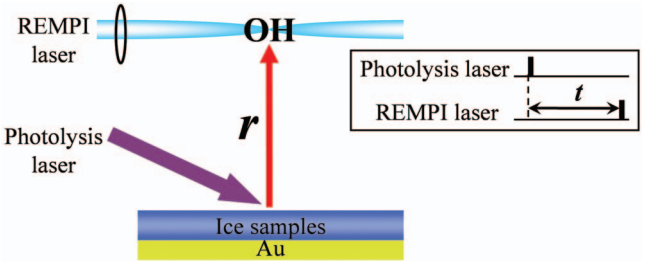

FIG. 1. Schematic illustration of the experiment. OH photofragments from the 157 nm photodissociation of water ice samples are detected by the REMPI technique. The timing plot for measurement of a time-of-flight (TOF) spectrum is shown in the inset where the delay time t between photolysis and probe laser pulses corresponds to the TOF. r(=2 mm) is the vertical distance between the disc substrate and the detection point. The 157 nm photoirradiated area is a disc with a radius of 6 mm.

For the H_2O_2/H_2O codeposited ice photolysis experiments, a commercially available H_2O_2 solution (30%) was concentrated in a glass container by vacuum distillation and the H_2O_2/H_2O vapor was deposited on ASW. The exposure of the H_2O_2/H_2O mixture on ASW was <10 L for 330 s duration at 90 K. Fresh surfaces of H_2O_2 cocondensed on ASW were prepared as described above.

All of present photolysis experiments were performed at a sample temperature of 90 K, and the chamber pressure was 5×10^{-7} Torr (due to the H_2O or H_2O_2/H_2O vapor injection into the chamber).

B. Simulation of time-of-flight spectra of OH products and REMPI transition factors

Time-of-flight (TOF) spectra of OH photoproducts were taken as a function of time t between the photolysis and REMPI laser pulses using a delay generator (Stanford Research) in order to investigate the flight times (and thus translational energies) of the desorbing OH photoproducts, as shown schematically in Fig. 1. Details regarding the simulation of such TOF spectra have been reported previously.[23,26] The measured TOF spectra $S(a_i,t,T_{trans})$ of the OH products were fitted to a sum of one or more flux-weighted Maxwell–Boltzmann (MB) distributions S_{MB}, each defined by a translational temperature T_{trans}. The coefficients a_i define the relative population associated with each MB component,

$$S(a_i,t,T_{trans}) = \Sigma a_i S_{MB}(t,T_{trans}), \quad (7)$$

$$S_{MB}(t,T_{trans}) = r^3 t^{-4} \exp[-mr^2/2k_B T_{trans} t^2], \quad (8)$$

$$P_{MB}(E_t) = (k_B T_{trans})^{-2} E_t \exp[-E_t/k_B T_{trans}], \quad (9)$$

where r is the distance between the substrate surface and the REMPI probe region. The MB distribution $P_{MB}(E_t)$ as a function of translational energy E_t is characterized by the

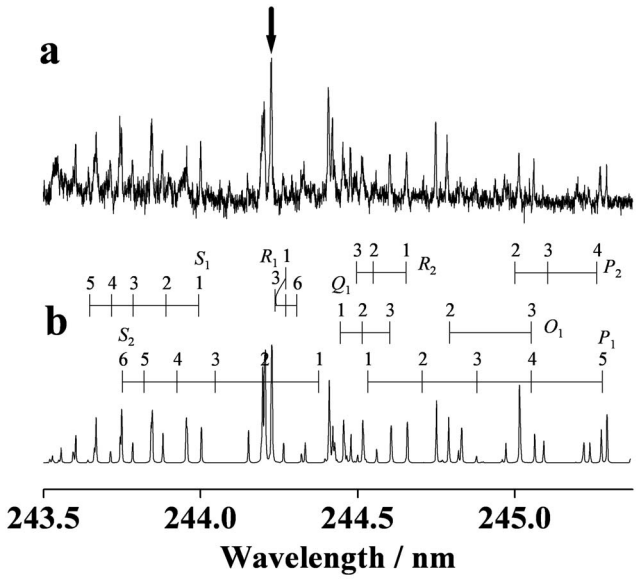

FIG. 2. (a) REMPI excitation spectrum of the OH $D\,^2\Sigma^- \leftarrow X\,^2\Pi$ $(v'=0,\ v''=0)$ transition from fresh ASW. TOF=1.5 μs. (b) A simulated OH spectrum assuming a Boltzmann distribution with $T_{rot}=400$ K. The arrow is the $R(1)+R(5)$ line used for TOF spectrum measurements.

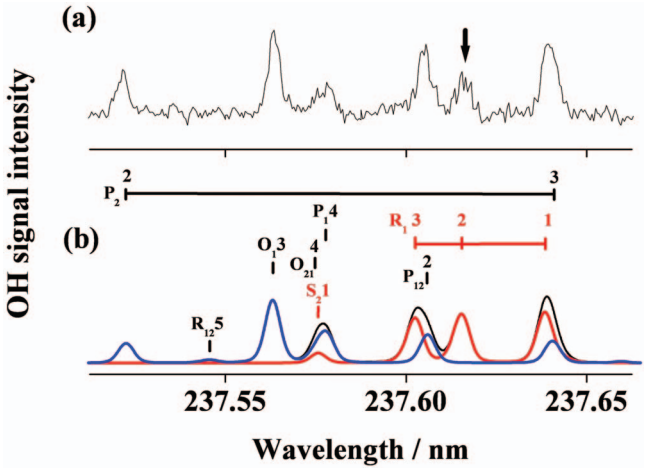

FIG. 3. (a) REMPI excitation spectrum of OH $D\,^2\Sigma^- \leftarrow X\,^2\Pi(v'=1,\ v''=0)$ and $3\,^2\Sigma^- \leftarrow X\,^2\Pi(v'=0,\ v''=1)$. TOF=1.5 μs. (b) A simulated spectrum assuming $T_{rot}(v=0)=400$ K (blue line) and $T_{rot}(v=1)=300$ K (red line). The experimental conditions are the same as for Fig. 2. The arrow is the $R(2)$ line used for TOF spectrum measurements.

averaged translational energy $\langle E_t\rangle = 2k_B T_{trans}$, where k_B is the Boltzmann constant.[27]

Model calculations were performed as follows. First, $P_{MB}(E_t)$ is converted from the energy distribution to the TOF distribution using the Jacobian listed by Zimmerman and Ho.[28] In these calculations we assume that signals come from a disc (vuv photoirradiation area) with a radius of 6 mm. Hence, an effective flight length is given by $(r^2+R^2)^{1/2}$ and the detection probability is proportional to $2\pi RdR/(r^2+R^2)$. We used $r=2$ mm and $0\leq R\leq 6$ mm. For the angular distribution of the photofragments from the ice surface, $\cos^n\theta$, where θ is the surface polar coordinate, $n=0$ was adopted in the best-fitting procedures because the parent H_2O or H_2O_2 molecules adsorb randomly on the ASW surfaces.[23,26] PGOPHER, a program for simulating rotational structure, was used.[29] The REMPI signals measured at a constant laser power were corrected by the constants for the respective electronic states of OH.[25,30]

III. RESULTS

A. OH radical from the 157 nm photolysis of fresh amorphous solid water

Figure 2(a) shows a REMPI spectrum of OH$(v=0)$ recorded at a fixed delay of $t=1.5$ μs, corresponding to the peak in the TOF profile from the 157 nm photolysis of fresh ASW. The rotational temperature $T_{rot}(v=0)$ is estimated to be 400 ± 100 K by spectral simulation [Fig. 2(b)]. Figure 3(a) shows a mixed band REMPI spectrum of OH ($v=0$ and 1) at $t=1.5$ μs. Figure 3(b) is a simulated mixed band spectrum for $T_{rot}(v=0)=400$ K and $T_{rot}(v=1)=300$ K. The rotational temperature $T_{rot}(v=1)$ is estimated to be 300 ± 100 K and the population ratio of $v=1/v=0$ is 0.2 ± 0.1 by spectral simulation. Figure 4(a) shows a typical TOF spectrum of OH$(v=0)$ for the $R(1)+R(5)$ line, which is reproduced by two MB distributions with $T_{trans}(v=0)=7500\pm1000$ K (5% contribution) and 1300 ± 300 K (95%). Figure 4(b) shows a typical TOF spectrum of OH$(v=1)$ for $R(2)$ line, which is reproduced with $T_{trans}(v=1)=7500\pm1000$ K (10%) and 1300 ± 300 K (90%). We found no clear evidence of the formation of vibrationally

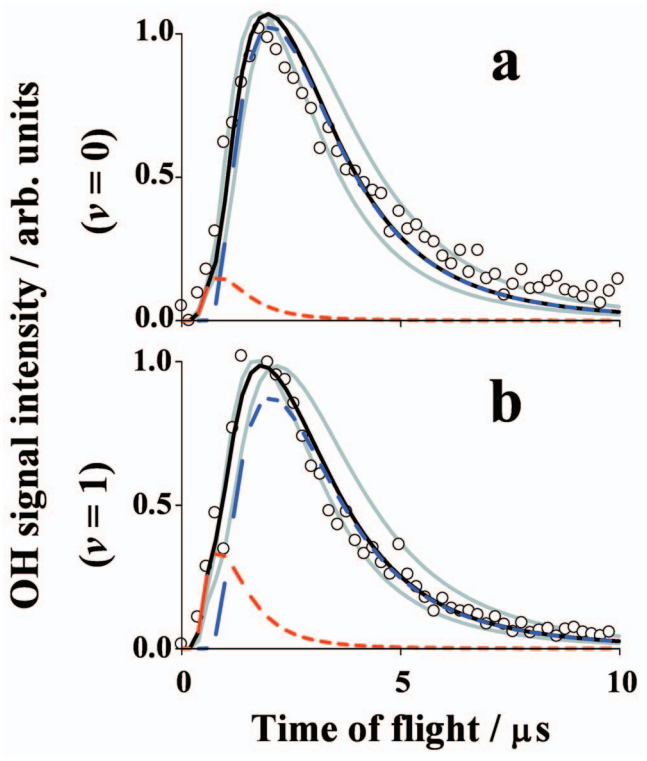

FIG. 4. (a) TOF spectrum of the $R(1)+R(5)$ line in the OH $D\,^2\Sigma^- \leftarrow X\,^2\Pi(v'=0,\ v''=0)$ transition. (b) $R(2)$ line in OH $3\,^2\Sigma^- \leftarrow X\,^2\Pi(v'=0,\ v''=1)$. The solid black curves are fits to the data derived assuming a MB distribution. (a) $T_{trans}=7500$ K (5% contribution, dashed red line) and 1300 K (95%, dashed blue line) and (b) $T_{trans}=7500$ K (10%) and 1300 K (90%). Other gray curves show the error bar ranges (see Table I). The experimental conditions are the same as for Fig. 2.

TABLE I. Contributions (percent) of translational and rotational temperature components of OH($v=0,1$) products.

	$v=0$		$v=1$		
	T_{trans} (K)	T_{rot} (K)	T_{trans} (K)	T_{rot} (K)	Population ratio $v=1/v=0$
Fresh ASW	7500 ± 1000 (5%)		7500 ± 1000 (10%)		
	1300 ± 300 (95%)	400 ± 100 [a]	1300 ± 300 (90%)	300 ± 100 [a]	0.2 ± 0.1 [a]
ASW after 1 hr irradiation	7500 ± 1000 (30%)		7500 ± 1000 (40%)		
	1300 ± 300 (70%)	500 ± 100 [b]	1300 ± 300 (60%)	200 ± 100 [b]	0.2 ± 0.1 [b]
H_2O_2 on ASW	7500 ± 1000 (30%)		7500 ± 1000 (40%)		
	1300 ± 300 (70%)	500 ± 100 [b]	1300 ± 300 (60%)	200 ± 100 [b]	0.2 ± 0.1 [b]
H_2O (gas phase)[c]	~1600	600	···	450	0.56–1.11[d]
Calculation for water ice[e]					0.3–0.5

[a]TOF=1.5 μs.
[b]TOF=0.5 μs.
[c]Reference 31.
[d]References 32 and 33.
[e]References 17 and 18.

excited OH($v=2$) in the wavelength region of the $3\ ^2\Sigma^-(v'=0) \leftarrow X\ ^2\Pi(v''=2)$ transition. Table I summarizes these results.

B. OH radical from the 157 nm photolysis of fresh H_2O_2 cocondensed on amorphous solid water

Figure 5 shows the typical TOF spectra of (a) OH ($v=0$) and (b) OH($v=1$) from the 157 nm photodissociation of fresh H_2O_2 cocondensed on ASW. The OH signal intensities were 1.5–1.8 times stronger than those from fresh ASW.

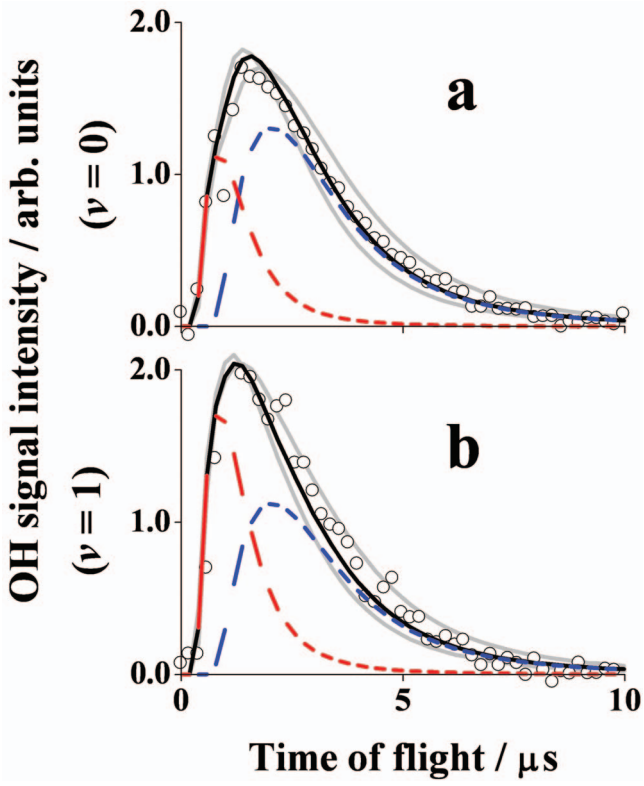

FIG. 5. (a) TOF spectrum of the $R(1)+R(5)$ line in OH $D\ ^2\Sigma^- \leftarrow X\ ^2\Pi(v'=0,\ v''=0)$ from fresh H_2O_2 cocondensed on ASW. (b) The $R(2)$ line in OH $3\ ^2\Sigma^- \leftarrow X\ ^2\Pi(v'=0,\ v''=1)$. The solid black curves are fits assuming (a) T_{trans}=7500 K (30%) and 1300 K (70%) and (b) T_{trans}=7500 K (40%) and 1300 K (60%). Other gray curves show the error bar ranges (see Table I).

These TOF spectra are reproduced by two MB distributions with $T_{trans}(v=0)=7500\pm1000$ K (30%) and 1300 ± 300 K (70%) and $T_{trans}(v=1)=7500\pm1000$ K (40%) and 1300 ± 300 K (60%). Figure 6(a) shows a REMPI spectrum of OH($v=0$) at $t=0.5$ μs, and $T_{rot}(v=0)$ is estimated to be 500 ± 100 K by spectral simulation [Fig. 6(c)]. Figure 7(a) shows a mixed band REMPI spectrum of OH ($v=0$ and 1) at $t=0.5$ μs. $T_{rot}(v=1)$ is estimated to be 200 ± 100 K and the population ratio $v=1/v=0$ is 0.2 ± 0.1 by spectral simulation [Fig. 7(c)]. Table I summarizes these results.

C. OH formation from the 157 nm photolysis of amorphous solid water after prolonged 157 nm irradiation

Figure 8 shows the TOF spectra of (a) OH($v=0$) and (b) OH($v=1$) formed by 157 nm photolysis of ASW, which were measured after 1 h photoirradiation without the intermissive

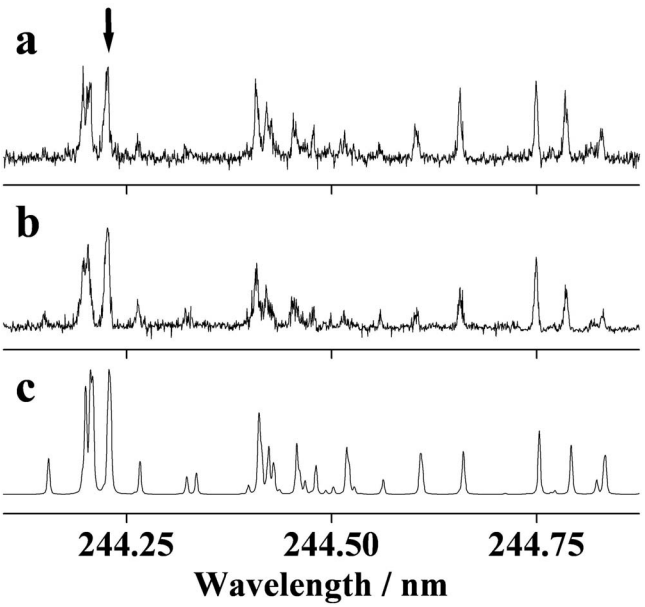

FIG. 6. REMPI excitation spectra of OH $D\ ^2\Sigma^- \leftarrow X\ ^2\Pi(v'=0,\ v''=0)$ of the fast OH signal (TOF=0.5 μs) from (a) fresh H_2O_2 (refer to Fig. 5). (b) After 1 h photoirradiation at 157 nm to ASW (refer to Fig. 8). (c) A simulated spectrum assuming T_{rot}=500 K.

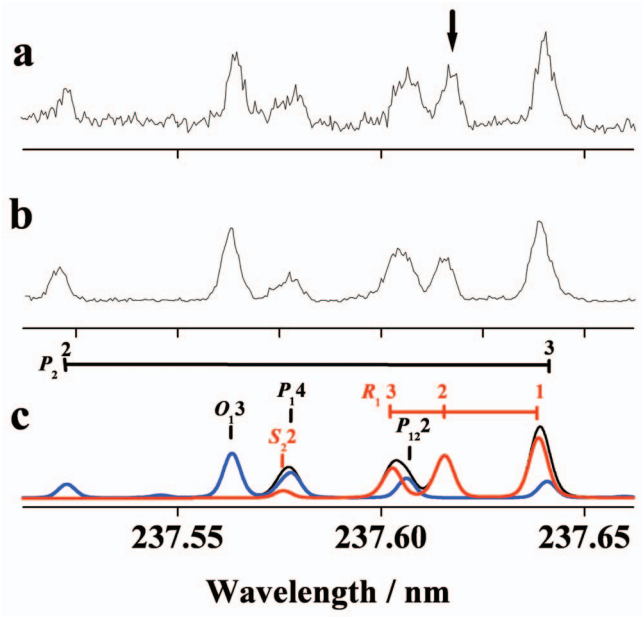

FIG. 7. REMPI excitation spectra of $D\ ^2\Sigma^- \leftarrow X\ ^2\Pi(v'=1,\ v''=0)$ and $3\ ^2\Sigma^- \leftarrow X\ ^2\Pi(v'=0,\ v''=1)$ of the fast OH signal (TOF=0.5 μs) from (a) fresh H_2O_2 (refer to Fig. 5). (b) After 1 h photoirradiation at 157 nm to an ASW film (refer to Fig. 8). (c) A simulated spectrum assuming $T_{rot}(v=0)=500$ K and $T_{rot}(v=1)=200$ K.

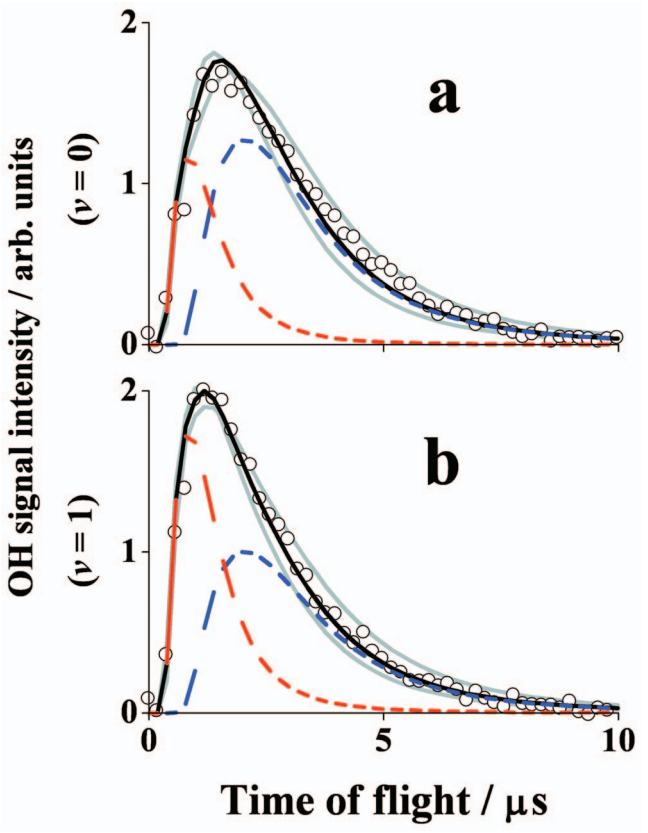

FIG. 8. (a) TOF spectrum of the $R(1)+R(5)$ line in OH $D\ ^2\Sigma^- \leftarrow X\ ^2\Pi$ $(v'=0,\ v''=0)$ from ASW after 1 h photoirradiation at 157 nm. (b) The $R(2)$ line in OH $3\ ^2\Sigma^- \leftarrow X\ ^2\Pi(v'=0,\ v''=1)$. The solid black curves are fits to the data derived assuming (a) $T_{trans}=7500$ K (30%) and 1300 K (70%) and (b) $T_{trans}=7500$ K (40%) and 1300 K (60%). Other gray curves show the error bar ranges (see Table I).

dosing of H_2O vapor. Without intermissive deposition of water vapor on the ASW surface after each laser shot, photoproducts are accumulated on/in ASW, and hence, the secondary photolysis of the H_2O_2 photoproducts becomes appreciable in the OH formation.[17] The OH signal intensity became about two times stronger than that from fresh ASW after prolonged photoirradiation because OH is produced from both the H_2O_2 and ASW photolysis. The contribution of the high translational temperature component ($T_{trans}=7500$ K) due to reaction (6) becomes appreciable. The results for translational temperatures and contributions are summarized in Table I.

To verify that the OH ($T_{trans}=7500$ K) component after prolonged 157 nm photoirradiation of ASW came from the photodissociation of the H_2O_2 photoproduct, time evolution curves of the OH($v=0$) and OH($v=1$) signal intensities were measured as a function of 157 nm irradiation time for the fast ($t=0.5$ μs) and slow ($t=2.5$ μs) TOF components. Figure 9 shows the results, in which OH signal intensities at $t=0$ are subtracted to show the increments caused by accumulated species due to prolonged irradiation at 157 nm . Figure 9 also includes the previously reported time evolution of H_2O_2 that was photolytically accumulated on the ASW surface by 157 nm irradiation.[17] The two appearance curves correspond with each other, suggesting that the source of OH after prolonged 157 nm irradiation is photochemically produced H_2O_2.

Figure 6(b) shows the REMPI spectrum of OH($v=0$) at $t=0.5$ μs and $T_{rot}=500\pm100$ K by spectral simulation [Fig. 6(c)]. Figure 7(b) shows a mixed band REMPI spectrum of OH ($v=0$ and 1) at $t=0.5$ μs with $T_{rot}(v=1)=200\pm100$ K. The population ratio of $v=1/v=0$ was 0.2 ± 0.1 by spectral simulation [Fig. 7(c)]. These results are almost the same as for H_2O_2 cocondensed on ASW described in Sec. III B, suggesting again that the source of OH after prolonged 157 nm irradiation is photochemically accumulated H_2O_2.

IV. DISCUSSION

A. Translational and internal energies of OH radicals from fresh amorphous solid water

The translational energies of OH($v=0$) and OH($v=1$) from fresh ASW are mostly fitted with a temperature $T_{trans}=1300\pm300$ K. This temperature (translational energy$=5.2\pm1.2$ kcal/mol) is in accordance with ~1600 K that was reported in the gas phase photodissociation of water at 157 nm by Mikulecky *et al.*[31] and the MD calculations (4.5–6.0 kcal/mol) by Andersson and co-workers.[18,19] A small contribution (5%–10%) of the fast ($T_{trans}=7500$ K) component would be due to the secondary photoprocess from the H_2O_2 products on ASW since the ASW surface was not completely covered with fresh H_2O vapor even with intermissive H_2O deposition. The rotational temperatures $T_{rot}(v=0)=400$ K and $T_{rot}(v=1)=300$ K are not thermally equilibrated with the ice film temperature of 90 K. Mikulecky *et al.*[31] reported $T_{rot}(v=0)=620$ K and $T_{rot}(v=1)=460$ K for OH formed from the gas phase photodissociation of H_2O. These results suggest that we observed nascent OH photofragments originated from the ASW surface.

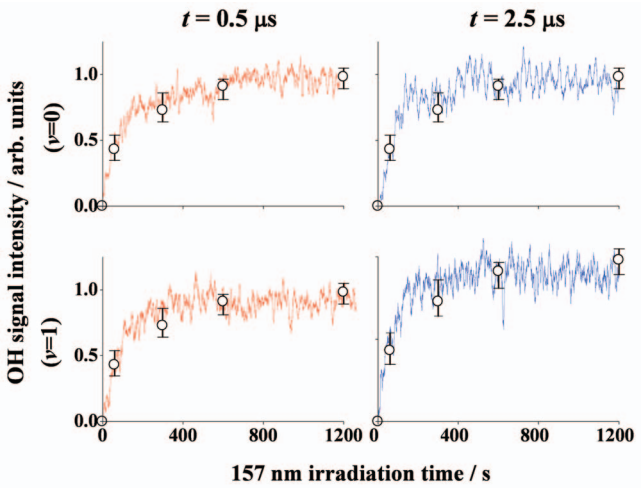

FIG. 9. Time evolution curves of the fast (t=0.5 μs) and slow (t=2.5 μs) components of OH [$R(1)+R(5)$ for $v=0$ and $R(2)$ for $v=1$] signals from ASW as a function of 157 nm irradiation time. OH signal intensities at $t=0$ are subtracted to show the increments caused by accumulated species due to 157 nm irradiation. Open circles represent the previously reported values for accumulation of H_2O_2 on ASW (Ref. 17).

Andersson and co-workers[18,19] calculated the desorption probabilities for OH radicals from water ice per absorbed vuv photon in the top 6 monolayers (ML). This gave the OH desorption probability as function of the monolayer in which H_2O was excited. Only a small fraction of OH radicals from the top 3 ML can desorb with desorption probability less than 3% per ML, while most OH products are trapped in/on the ice at 10 K. The lack of a surface accommodated TOF component in the present results indicates that OH formed in the ice bulk is readily trapped or reacts with water molecules in the ice bulk. In addition, the rotational distribution is essentially the same as those observed and calculated for gas-phase H_2O photolysis. We conclude that the dominant fraction of OH desorbed into vacuum is released from the topmost monolayer(s) of ASW.

Our present observation of vibrational distribution $v=1/v=0\approx 0.2$ is in fair agreement with the molecular dynamic calculations at 10 K by Andersson and co-workers,[18,19] which predicted that desorbed OH has a maximum population at $v=0$ and that the amount of vibrational excitation drops only by about 30%–50% from one excited level to the next. The fractions of the total available energy partitioned into the different degrees of freedom in the dissociation products have also been determined. Using the translational, vibrational, and rotational distributions, it was found that 8%–12% of the available energy (51.2 kcal/mol) was partitioned into translation, 5%–7% into vibration, and 1% and 2% into rotation. The remainder presumably has been partitioned into the ASW matrix and translational energy of the H atom.

It is interesting to note the difference between the gas phase and solid phase photodynamics for H_2O at 157 nm. Hwang *et al.*[32] and Yang *et al.*[33] showed that OH($v=1$) was populated by 10% more than OH($v=0$), and OH($v\geq 2$) populations dropped below the detection threshold. This vibrational state distribution is different from the condensed phase results as presented in this paper. Reasons for this can be found in differences in the excited state potentials, dissipation of energy, and/or the dynamics of the photodissociation process. The two first cases were already discussed in some depth by Andersson and co-workers.[18,19] In short, there is evidence that the surrounding water molecules affect the electronically excited state of H_2O by lowering the intramolecular part of the excitation energy. This was also found in the high-level electronic structure calculations by Chipman,[34,35] which showed that the first excited state potential energy surface of H_2O is significantly affected by neighboring H_2O molecules. This would lead to somewhat different product energy distributions.

The translational energy distribution of the desorbing H atoms seemed to be affected by this effect, possibly combined with the dissipation of excess energy.[14] This dissipation of energy will most likely proceed through energy transfer to vibrational modes of water molecules in the ice and/or through reaction of energetic H atoms with H_2O,[14–16]

$$H + H_2O \rightarrow H_2 + OH. \quad (10)$$

The good agreement between the classical MD calculations and experiments could be fortuitous or there could be a more fundamental reason for this. Generally, full quantum dynamics calculations are required to obtain reliable product quantum state distributions. This has been done for the case of gas-phase photodissociation of H_2O by van Harrevelt and van Hemert.[36] However, in the case of multidimensional systems such as a liquid or a solid the most important quantum effects are often "static," i.e., inclusion of zero-point energy, rather than dynamic interference effects.[37,38] The reason for this is the rapid loss of coherence that is common in condensed phases.

B. OH radical formation by the secondary photoprocess of H_2O_2

In their MD calculations, Andersson and co-workers[18,19] studied the mobility of OH radicals following the photolysis of water ice. The OH radicals formed in the ice move only at a maximum distance of 5 Å at 10 K. However, OH radicals formed from photodissociation in the top 3 ML are able to move up to more than 60 Å. This indicates that the OH radicals that have diffused along the surface and have dissipated some of their internal energy to the surface in the process are likely trapped at the surface site but not desorbed. On the other hand, Petrik *et al.*[13] reported the low-energy electron-stimulated production of molecular oxygen from thin ASW films and proposed that the electron-stimulated migration of OH or OH^- to the vacuum interface, where they react and produce molecular oxygen, occurs via transport through the hydrogen bond network of the ASW. In either case, it is speculated that the recombination of OH to form H_2O_2 occurs more readily at the surface of ASW compared to the bulk. In fact, Yabushita *et al.*[17] reported in their vuv photolysis experiments that H_2O_2 was subsequently produced on the water ice surface at 90 K presumably due to recombination of photolytically produced OH.

Figure 9 shows the appearance behavior of OH signals mainly due to reaction (6), the secondary photodissociation

of surface-bound H_2O_2 formed via reaction (3). The higher-translational temperature (T_{trans}=7500 K) of Figs. 5(a) and 5(b) is attributed to the larger E_{avail} in reaction (6) than reaction (5). In addition, the translational and internal energies for the OH radicals from H_2O_2 directly condensed on ASW are in good accordance with those for the OH radicals following the prolonged 157 nm irradiation of ASW. Therefore, the contribution of OH radicals from other by-products such as HO_2 formed as follows would be small, since (a) HO_2 is produced from a three-step reaction of $OH+H_2O_2$, where H_2O_2 is produced from OH+OH, and (b) HO_2 disappears at elevated temperatures,[7]

$$H_2O_2 + h\nu \rightarrow H + HO_2, \quad (11)$$

$$H_2O_2 + OH \rightarrow H_2O + HO_2, \quad (12)$$

$$HO_2 + h\nu \rightarrow O + OH. \quad (13)$$

V. CONCLUSION

In the 157 nm irradiation experiments on ASW at 90 K, we have measured the translational and rotational temperatures and vibrational distributions for OH (v=0 and 1) that are the products from surface H_2O of ASW as well as the products from H_2O_2 that is photochemically produced on the surface of ASW. OH from H_2O is characterized by a translational temperature of 1300 K, while that of OH from H_2O_2 is 7500 K. We found that the contribution of the secondary photolysis of accumulated photoproducts is appreciable in the condensed phase photoprocesses of water ice.

ACKNOWLEDGMENTS

This work is supported by a grant in aid from JSPS (Grant No. 20245005).

[1] V. Poterya, M. Fárník, M. Ončák, and P. Slavíček, Phys. Chem. Chem. Phys. **10**, 4835 (2008).
[2] J. D. Thrower, M. P. Collings, M. R. S. McCoustra, D. J. Burke, W. A. Brown, A. Dawes, P. D. Holtom, P. Kendall, N. J. Mason, F. Jamme, H. J. Fraser, I. P. Clark, and A. W. Parker, J. Vac. Sci. Technol. A **26**, 919 (2008).
[3] C. L. Thomsen, D. Madsen, S. R. Keiding, J. Thøgersen, and O. Christiansen, J. Chem. Phys. **110**, 3453 (1999).
[4] M. Seki, K. Kobayashi, and J. Nakahara, J. Phys. Soc. Jpn. **50**, 2643 (1981).
[5] L. J. Stief, W. A. Payne, and R. B. Klemm, J. Chem. Phys. **62**, 4000 (1975).
[6] A. A. Y. M. Ung, Chem. Phys. Lett. **28**, 603 (1974).
[7] P. A. Gerakines, W. A. Schutte, and P. Ehrenfreund, Astron. Astrophys. **312**, 289 (1996).
[8] J. A. Ghormley and C. J. Hochanadel, J. Phys. Chem. **75**, 40 (1971).
[9] M. S. Westley, R. A. Baragiola, R. E. Johnson, and G. A. Baratta, Nature (London) **373**, 405 (1995).
[10] M. S. Westley, R. A. Baragiola, R. E. Johnson, and G. A. Baratta, Planet. Space Sci. **43**, 1311 (1995).
[11] G. A. Kimmel and T. M. Orlando, Phys. Rev. Lett. **75**, 2606 (1995).
[12] G. A. Kimmel, R. G. Tonkyn, and T. M. Orlando, Nucl. Instrum. Methods Phys. Res. B **101**, 179 (1995).
[13] N. G. Petrik, A. G. Kavetsky, and G. A. Kimmel, J. Chem. Phys. **125**, 124702 (2006).
[14] A. Yabushita, D. Kanda, N. Kawanaka, M. Kawasaki, and M. N. R. Ashfold, J. Chem. Phys. **125**, 133406 (2006).
[15] A. Yabushita, T. Hama, D. Iida, N. Kawanaka, M. Kawasaki, N. Watanabe, M. N. R. Ashfold, and H. P. Loock, Astrophys. J. **682**, L69 (2008).
[16] A. Yabushita, T. Hama, D. Iida, N. Kawanaka, M. Kawasaki, N. Watanabe, M. N. R. Ashfold, and H. P. Loock, J. Chem. Phys. **129**, 044501 (2008).
[17] A. Yabushita, T. Hama, D. Iida, and M. Kawasaki, J. Chem. Phys. **129**, 014709 (2008).
[18] S. Andersson, A. Al-Halabi, G. J. Kroes, and E. F. van Dishoeck, J. Chem. Phys. **124**, 064715 (2006).
[19] S. Andersson and E. F. van Dishoeck, Astron. Astrophys. **491**, 907 (2008).
[20] K. I. Öberg, H. Linnartz, R. Visser, and E. F. van Dishoeck, Astrophys. J. **693**, 1209 (2009).
[21] M. Kh. Karapet'yants and M. K. Karapet'yants, *Handbook of Thermodynamic Constants of Inorganic and Organic Compounds* (Humphrey Science Publishers, Ann Arbor, 1970).
[22] A. J. Matich, M. G. Bakker, D. Lennon, T. I. Quickenden, and C. G. Freeman, J. Phys. Chem. **97**, 10539 (1993).
[23] A. Yabushita, Y. Inoue, T. Senga, M. Kawasaki, and S. Sato, J. Phys. Chem. B **106**, 3151 (2002).
[24] M. Kawasaki, Appl. Surf. Sci. **135**, 115 (1998).
[25] M. E. Greenslade, M. I. Lester, D. C. Radenovic, A. J. A. van Roij, and D. H. Parker, J. Chem. Phys. **123**, 074309 (2005).
[26] A. Yabushita, Y. Inoue, T. Senga, M. Kawasaki, and S. Sato, J. Phys. Chem. A **108**, 438 (2004).
[27] F. M. Zimmermann and W. Ho, J. Chem. Phys. **100**, 7700 (1994).
[28] F. M. Zimmermann and W. Ho, Surf. Sci. Rep. **22**, 127 (1995).
[29] C. M. Western, PGOPHER, a program for simulating rotational structure, University of Bristol, http://pgopher.chm.bris.ac.uk.
[30] K. P. Huber and G. Herzberg, *Molecular Spectra and Molecular Structure IV. Constants of Diatomic Molecules* (Van Nostrand Reinhold, New York, 1979).
[31] K. Mikulecky, K. H. Gericke, and F. J. Comes, Chem. Phys. Lett. **182**, 290 (1991).
[32] D. W. Hwang, X. F. Yang, and X. M. Yang, J. Chem. Phys. **110**, 4119 (1999).
[33] X. F. Yang, D. W. Hwang, J. J. Lin, and X. Ying, J. Chem. Phys. **113**, 10597 (2000).
[34] D. M. Chipman, J. Chem. Phys. **122**, 044111 (2005).
[35] D. M. Chipman, J. Chem. Phys. **124**, 044305 (2006).
[36] R. van Harrevelt and M. C. van Hemert, J. Chem. Phys. **114**, 9453 (2001).
[37] J. A. Poulsen, G. Nyman, and P. J. Rossky, Proc. Natl. Acad. Sci. U.S.A. **102**, 6709 (2005).
[38] J. A. Poulsen, G. Nyman, and P. J. Rossky, J. Chem. Theory Comput. **2**, 1482 (2006).